REPORT DOCUMENTATION PAGE

1

Form Approved OMB NO. 0704-0188

1. REPORT DATE (DD-MM-YYYY)	2. REPORT TYPE	3. DATES COVERED (From - To)
22-09-2014	Final Report	17-Sep-2012 - 16-Jun-2014

4. TITLE AND SUBTITLE
Final Report: Self-Assembly of Reconfigurable By-Design Optical Materials with Molecular-Level Control

5a. CONTRACT NUMBER
W911NF-12-1-0581

5b. GRANT NUMBER

5c. PROGRAM ELEMENT NUMBER
611102

6. AUTHORS
Wounjhang Park; Wei Zhang

5d. PROJECT NUMBER

5e. TASK NUMBER

5f. WORK UNIT NUMBER

7. PERFORMING ORGANIZATION NAMES AND ADDRESSES
University of Colorado - Boulder
3100 Marine Street, Room 479
572 UCB
Boulder, CO 80303 -1058

8. PERFORMING ORGANIZATION REPORT NUMBER

9. SPONSORING/MONITORING AGENCY NAME(S) AND ADDRESS (ES)
U.S. Army Research Office
P.O. Box 12211
Research Triangle Park, NC 27709-2211

10. SPONSOR/MONITOR'S ACRONYM(S)
ARO

11. SPONSOR/MONITOR'S REPORT NUMBER(S)
61974-MS.3

12. DISTRIBUTION AVAILIBILITY STATEMENT
Approved for Public Release; Distribution Unlimited

13. SUPPLEMENTARY NOTES
The views, opinions and/or findings contained in this report are those of the author(s) and should not contrued as an official Department of the Army position, policy or decision, unless so designated by other documentation.

14. ABSTRACT
Artificial structured materials hold high promise of providing a path to by-design optical materials with engineered optical properties. One of the major roadblocks for practical applications is the lack of efficient fabrication technology, which is also one of the grand challenges in nanotechnology in general. An efficient and scalable technique capable of producing large-area, three-dimensional (3D) structures is critically needed and self-assembly of nanoparticles offers an attractive solution to this problem. While there have been many studies on self-assembly of nanomaterials, precise molecular-level control of the assembly process over a large area or volume is yet to

15. SUBJECT TERMS
Self-Assembly, Molecular Cage, Plasmonics

16. SECURITY CLASSIFICATION OF:			17. LIMITATION OF ABSTRACT	15. NUMBER OF PAGES	19a. NAME OF RESPONSIBLE PERSON
a. REPORT	b. ABSTRACT	c. THIS PAGE			Wounjhang Park
UU	UU	UU	UU		19b. TELEPHONE NUMBER 303-735-3601

Report Title

Final Report: Self-Assembly of Reconfigurable By-Design Optical Materials with Molecular-Level Control

ABSTRACT

Artificial structured materials hold high promise of providing a path to by-design optical materials with engineered optical properties. One of the major roadblocks for practical applications is the lack of efficient fabrication technology, which is also one of the grand challenges in nanotechnology in general. An efficient and scalable technique capable of producing large-area, three-dimensional (3D) structures is critically needed and self-assembly of nanoparticles offers an attractive solution to this problem. While there have been many studies on self-assembly of nanomaterials, precise molecular-level control of the assembly process over a large area or volume is yet to achieved. Here, we report a new approach to plasmonic nanoparticle self-assembly based on 3D shape-persistent cage molecules. Well-defined, rigid, 3D purely organic cage-like molecules have attracted great research attention due to their unique shape-persistency, structure-tunability, and chemical and thermal stability. However, to the best of our knowledge, utilizing rigid cage molecules as linkers to control the nanoparticle assembly has not yet been explored. The modular construction of cage molecules provides the design flexibility required to control the nanoparticle assembly process. Also, the shape-persistent nature of the molecules leads to highly stable and robust structures. In the following, we report successful self-assembly of gold nanoparticles using two different types of cage molecules as linkers. Our results shed light on how the molecular structures affect and thus can be used to control the self-assembly process.

Enter List of papers submitted or published that acknowledge ARO support from the start of the project to the date of this printing. List the papers, including journal references, in the following categories:

(a) Papers published in peer-reviewed journals (N/A for none)

Received		Paper
08/20/2013	1.00	Wounjhang Park, Kazunori Emoto, Yinghua Jin, Akihiro Shimizu, Venkata A. Tamma, Wei Zhang. Controlled self-assembly of gold nanoparticles mediated by novel organic molecular cages, Optical Materials Express, (01 2013): 0. doi: 10.1364/OME.3.000205
09/22/2014	2.00	Ryan McCaffrey, Hai Long, Yinghua Jin, Aric Sanders, Wounjhang Park, Wei Zhang. Template Synthesis of Gold Nanoparticles with an Organic Molecular Cage, Journal of the American Chemical Society, (02 2014): 0. doi: 10.1021/ja412606t
TOTAL:		**2**

Number of Papers published in peer-reviewed journals:

(b) Papers published in non-peer-reviewed journals (N/A for none)

Received		Paper
TOTAL:		

Number of Papers published in non peer-reviewed journals: 3

(c) Presentations

W. Park, "Self-Assembly Based on Molecular Cages", The 5th International Conference on Metamaterials, Photonic Crystals and Plasmonics, Singapore, May 20 - 23, 2014.
Zhang, W. "Design, Synthesis, and Applications of Covalent Organic Nanocages", 246th ACS National Meeting & Exposition, Indianapolis, IN, United States, September 8-12, 2013 (2013), COLL-104.

Number of Presentations: 2.00

Non Peer-Reviewed Conference Proceeding publications (other than abstracts):

Received Paper

TOTAL:

Number of Non Peer-Reviewed Conference Proceeding publications (other than abstracts):

Peer-Reviewed Conference Proceeding publications (other than abstracts):

Received Paper

TOTAL:

Number of Peer-Reviewed Conference Proceeding publications (other than abstracts):

(d) Manuscripts

Received Paper

TOTAL:

Number of Manuscripts: 4

Books

Received Book

TOTAL:

Received Book Chapter

TOTAL:

Patents Submitted

Novel self-assembling nano composite structures and methods of preparing the same

Patents Awarded

Awards

Graduate Students

NAME	PERCENT_SUPPORTED	Discipline
Ryan McCaffrey	0.50	
Devin Rourke	0.50	
FTE Equivalent:	**1.00**	
Total Number:	**2**	

Names of Post Doctorates

NAME	PERCENT_SUPPORTED
FTE Equivalent:	
Total Number:	

Names of Faculty Supported

NAME	PERCENT_SUPPORTED	National Academy Member
Wounjhang Park	0.04	
Wei Zhang	0.04	
FTE Equivalent:	**0.08**	
Total Number:	**2**	

Names of Under Graduate students supported

NAME	PERCENT_SUPPORTED
FTE Equivalent:	
Total Number:	

Student Metrics

This section only applies to graduating undergraduates supported by this agreement in this reporting period

The number of undergraduates funded by this agreement who graduated during this period:	0.00
The number of undergraduates funded by this agreement who graduated during this period with a degree in science, mathematics, engineering, or technology fields:.....	0.00
The number of undergraduates funded by your agreement who graduated during this period and will continue to pursue a graduate or Ph.D. degree in science, mathematics, engineering, or technology fields:.....	0.00
Number of graduating undergraduates who achieved a 3.5 GPA to 4.0 (4.0 max scale):.....	0.00
Number of graduating undergraduates funded by a DoD funded Center of Excellence grant for Education, Research and Engineering:.....	0.00
The number of undergraduates funded by your agreement who graduated during this period and intend to work for the Department of Defense	0.00
The number of undergraduates funded by your agreement who graduated during this period and will receive scholarships or fellowships for further studies in science, mathematics, engineering or technology fields:	0.00

Names of Personnel receiving masters degrees

NAME
Total Number:

Names of personnel receiving PHDs

NAME
Total Number:

Names of other research staff

NAME	PERCENT_SUPPORTED
FTE Equivalent:	
Total Number:	

Sub Contractors (DD882)

Inventions (DD882)

Scientific Progress

See attachment.

Technology Transfer

Final Progress Report

Self-assembly of reconfigurable by-design optical materials with molecular-level control

Prepared by:

Wounjhang Park and Wei Zhang
University of Colorado Boulder

Prepared for:

Dr. John Prater
Army Research Office

Project Period Covered:

Sep. 17, 2012 ~ Jun. 15, 2014

Report Date:
Sept. 21, 2014

Table of contents

List of Illustrations

1. Problem Statements

Artificial structured materials such as photonic crystal and metamaterial hold high promise of providing a path to by-design optical materials with engineered optical properties. In the past decade, the field has seen an explosive growth fuelled by the demonstrations of novel properties like negative refractive index and invisibility. One of the major roadblocks for practical applications is the lack of efficient fabrication technology, which is also one of the grand challenges in nanotechnology in general. So far, vast majority of optical metamaterials have been fabricated by top-down techniques such as electron-beam lithography or focused ion beam milling. While these techniques provide powerful means to sculpt nanostructures with high precision, they are slow, expensive and generally limited to two-dimensional structures. An efficient and scalable technique capable of producing large-area, three-dimensional (3D) structures is critically needed and self-assembly of nanoparticles offers an attractive solution to this problem. While there have been many studies on self-assembly of nanomaterials, precise molecular-level control of the assembly process over a large area or volume is yet to achieved. Here, we report a new approach to plasmonic nanoparticle self-assembly based on 3D shape-persistent cage molecules. Well-defined, rigid, 3D purely organic cage-like molecules have attracted great research attention due to their unique shape-persistency, structure-tunability, and chemical and thermal stability. However, to the best of our knowledge, utilizing rigid cage molecules as linkers to control the nanoparticle assembly has not yet been explored. The modular construction of cage molecules provides the design flexibility required to control the nanoparticle assembly process. Also, the shape-persistent nature of the molecules leads to highly stable and robust structures. In the following, we report successful self-assembly of gold nanoparticles using two different types of cage molecules as linkers. Our results shed light on how the molecular structures affect and thus can be used to control the self-assembly process.

2. Self-assembly of gold nanoparticles by molecular cage linkers

The first self-assembly work was to use cage molecules as linkers to precisely control the interparticle spacing. It is noted that this work was started in the previous DARPA grant and was completed under the current project. As linkers, we designed, synthesized and investigated two different cage molecules, also called covalent organic polyhedrons (COP), tri(4-pyridyl)-substituted COP (**COP-3P**) and hexa(4-pyridylvinyl)-substituted COP (**COP-6VP**) along with a small ligand molecule, 1,3,5-tri(4-pyridylvinyl)benzene (**TP**), which was used as a reference compound. These molecules were chosen to provide insights into how the binding efficiency and kinetics are influenced by the cage structures on the molecular-level. As shown in Fig. 1, pyridyl groups were installed on all three molecules as anchoring sites for binding with gold nanoparticles. The binding between gold and pyridyl group is well characterized and widely used in many applications.[1-3] **TP** and **COP-3P** have three pyridyl groups whereas **COP-6VP** has six. Recent advances in dynamic covalent chemistry have enabled facile access to nanometer-sized covalently linked cage molecules from simple synthetic precursors.[4,5] As shown in Fig. 2, trigonal prismatic cage **COP-1** and **COP-2** were constructed through dynamic imine metathesis, in which the product formation was under thermodynamic control, from 2:3 equivalent of triamine and dialdehyde building units. Bromo functional groups were installed on each of the side arms as the synthetic handle for further introducing the nanoparticle binding sites. The pyridine binding sites were then installed through cross-coupling reaction of **COP-1** and **COP-2**

with pyridine-4-boronic acid and 4-vinylpyridine respectively to provide **COP-3P** and **COP-6VP**.

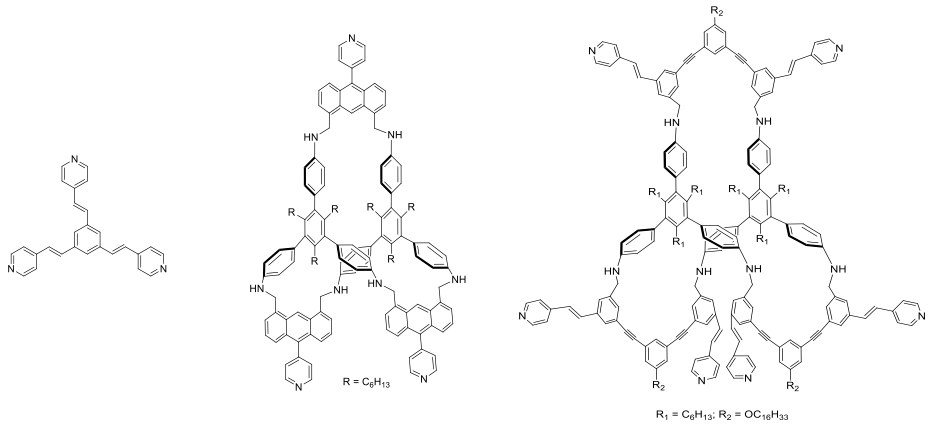

Figure 1. Schematic diagrams of molecules used for self-assembly of gold nanoparticles.

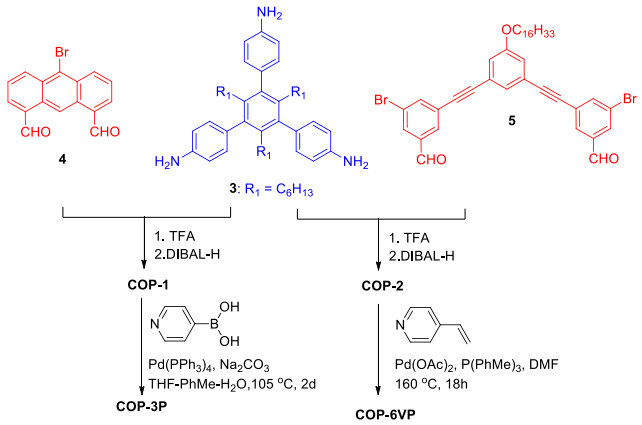

Figure 2. Synthesis of **COP-3P** and **COP-6VP**

Thanks to its small size (14.7Å), **TP** molecules can readily rotate and reorient themselves and thus bind with gold nanoparticles efficiently.[3] The COP molecules are larger and therefore not as nimble as **TP**. This difference was obvious when the gold nanoparticle solution and cage molecule solution were mixed for a quick test of binding kinetics. The original gold nanoparticle solution with an average particle size of 14 nm was red due to the strong surface plasmon absorption peak at 520 nm. When **TP** was added, the solution immediately turned purple. The optical extinction spectrum revealed the emergence of a second peak near 700 nm, which was due to the coupling between individual nanoparticle plasmon resonances. This observation was consistent with a previous report[3] and was a direct evidence of nanoparticle cluster formation and suggests highly efficient binding between **TP** ligand molecules and gold nanoparticles. For both **COP-3P** and **COP-6VP**, the solution color change occurred slowly over an hour or longer,

indicating the nanoparticle assembly was much slower. Furthermore, in contrast to **TP**, mixing gold nanoparticles with **COP-3P** or **COP-6VP**, only led to a slight red shift of absorption peak without showing the second peak near 700 nm on the UV-Vis spectrum, as shown in Fig. 3. These results were consistent with those from self-assembly and the mechanism behind this phenomenon is elucidated later.

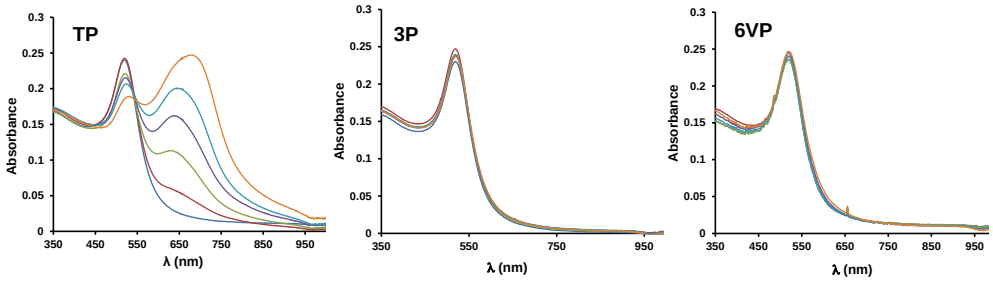

Figure 3. Titration study: **TP** (50 μM), **COP-3P** (50 μM), and **COP-6VP** (50 μM) in THF were added (0-25 μL in 5 μL increments) to aqueous solutions of AuNPs (0.5 mL). After mixing the components, they were diluted to 5 mL and the absorption spectra were recorded.

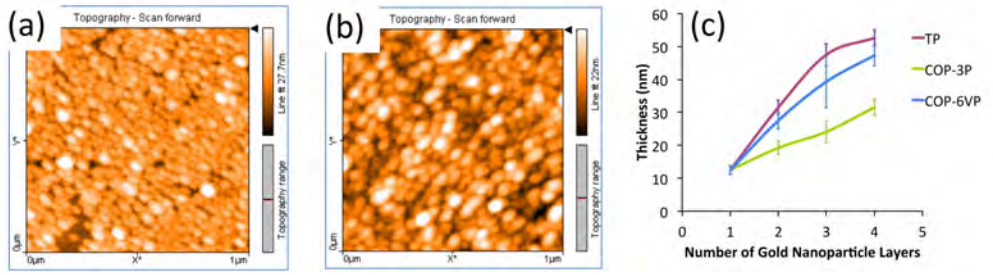

Figure 4. Topography scans obtained by AFM for (a) monolayer of gold nanoparticles and (b) 4 layers of gold nanoparticles self-assembled by **COP-3P** molecules. (c) Thickness measured by AFM as a function of the number of gold nanoparticle layers for self-assembly mediated by various molecules.

Self-assembly of gold nanoparticles were conducted in a layer-by-layer fashion similarly to what have been reported previously.[6,7] In this process, the first layer of gold nanoparticles on the substrate was formed by electrostatic interaction between the negatively charged gold nanoparticles in aqueous solution and the substrate surface positively charged by amine-functionalization. Atomic force microscopy (AFM) showed that a monolayer of high-density, well-dispersed gold nanoparticle was formed (Fig. 4a). The particle surface density was measured to be ~730 μm^{-2}, which was comparable to what has recently been reported for gold nanoparticle deposition via electrostatic interaction.[8] Due to the finite size of the AFM tip, the individual nanoparticle size in AFM images was 31 nm. The average center-to-center spacing between two neighboring nanoparticles was 37 nm. On top of the monolayer prepared this way, cage molecule solution and gold nanoparticle solution were applied sequentially by drop-casting method. After each cycle of sequential application of cage molecule solution and gold

nanoparticle solution to the self-assembly surface, the surface topography and layer thickness were measured by AFM. The AFM images generally showed a surface with well dispersed gold nanoparticles, as shown in the example of 4 layer gold nanoparticles self-assembled with **COP-3P** molecules in Fig. 4b. Although not shown, the surfaces of **TP** and **COP-6VP** mediated self-assembly exhibited similar topographies. As the number of layers of self-assembled nanoparticles was increased, the average particle size increased to 45~55 nm in diameter, indicating a small degree of clustering of nanoparticles on the self-assembly surface. However, the rms roughness remained small and lied between 3 and 6 nm in all samples, indicating uniform layer-by-layer assembly was accomplished. Particle surface density also remained stable between 800 and 1000 mm^{-2}.

To determine whether the gold nanoparticle layers were indeed assembled in layer-by-layer fashion, thickness was measured by AFM as the self-assembly was being carried out. As shown in Fig. 4c, the total gold nanoparticle layer thickness increased in all cases as more cycles of self-assembly were conducted, indicating that the gold nanoparticles were captured and bound to the growth surface by the linker molecules used for self-assembly. However, the thickness was substantially lower for the samples self-assembled with **COP-3P** molecules than other molecules. This was attributed to the inefficient binding between **COP-3P** and gold nanoparticles, which was expected from the molecular structure of **COP-3P**. As shown in Fig. 1, **COP-3P** had pyridyl binding groups rigidly attached to the cage frame. In contrast, **COP-6VP** had more flexible vinyl groups (through vinyl and phenyl C-C single bond rotation) linking the pyridyls to the cage frame, thereby providing rotational freedom to the binding groups. As a result, **TP** and **COP-6VP** molecules with flexible binding groups could bind much more efficiently with gold nanoparticles than **COP-3P** molecule. In the thickness data, the inefficient binding of **COP-3P** with gold nanoparticles manifested itself with lower thicknesses. For the other two molecules, **TP** and **COP-6VP**, the thicknesses were similar. The differences in thicknesses were 5~8 nm, which was substantially smaller than the single gold nanoparticle size, 14 nm. It could thus be stated that highly efficient binding with gold nanoparticles was achieved in both cases. While the thickness differences were small, the thickness was consistently larger with **TP** than **COP-6VP**. This result showed that there was some correlation between the molecule size and binding efficiency. **TP** was the smallest planer molecule and thus able to readily diffuse, rotate and reorient itself to bind with gold nanoparticles. This allowed high accessibility of ligand group to nanoparticles, leading a denser nanoparticle array on the surface. The larger size **COP-6VP** molecule was not as nimble as **TP** and consequently exhibited less efficient binding, which resulted in lower thicknesses than **TP**. However, despite the substantially larger size, **COP-6VP** resulted in thicknesses only slightly smaller than **TP**. This was because **COP-6VP** had a larger number (six) of binding groups than **TP** which had three.

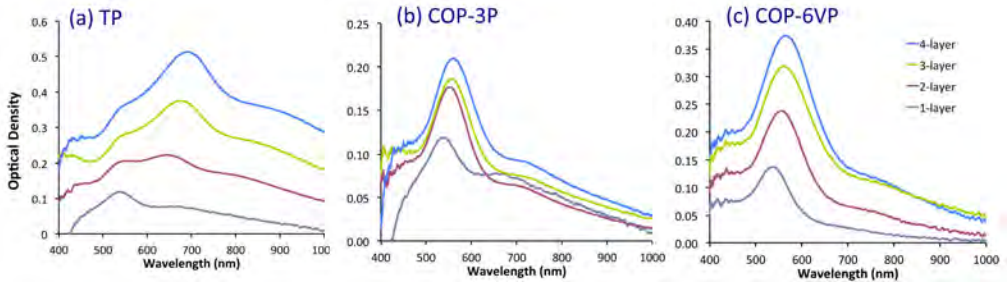

Figure 5. Optical extinction spectra for self-assembled gold nanoparticles using linker molecules (a) **TP**, (b) **COP-3P** and (c) **COP-6VP**.

Optical extinction spectroscopy was carried out for the self-assembled layers of gold nanoparticles. Fig. 5 show the extinction spectra of 1~4 layers of gold nanoparticles self-assembled with **TP**, **COP-3P**, and **COP-6VP** molecules. In all cases, the extinction increased as more layers were assembled. This was consistent with the thickness data which showed the thickness increased with increasing number of self-assembled layers with all three molecules. However, the peak extinction values showed significant differences depending on which molecule was used for self-assembly. **TP** resulted in the highest extinction and **COP-3P** gave the lowest with **COP-6VP** showing slightly lower extinction than **TP**. Since none of the linker molecules has absorption above 400 nm, the optical extinction in the visible spectrum should be proportional to the total number of gold nanoparticles present in the light path, which in our samples is determined by the thickness of the self-assembled layer and density of gold nanoparticles in it. The peak extinction observed in **TP**, **COP-3P** and **COP-6VP** samples was in excellent agreement with the thickness data obtained by AFM, once again confirming that **TP** led to the most efficient binding followed by **COP-6VP** and **COP-3P** in that order.

The optical extinction spectra offer another information on gold nanoparticle packing from the position of peak extinction. The origin of the extinction peak is obviously the surface plasmon resonance of gold nanoparticles. According to the Mie theory, a 14 nm size gold sphere placed on a glass substrate should exhibit extinction peak at around 530 nm, which was exactly what was observed from the monolayer samples as shown in Fig. 5. This confirms that the gold nanoparticles are uniformly distributed on the surface with minimal aggregations. As more gold nanoparticle layers were added by subsequent self-assembly processes, the surface plasmon resonances of individual gold nanoparticles couple together with those of neighboring nanoparticles and the resultant delocalization consequently leads to the lowering of resonance frequency and red shift in the optical extinction peak. The peak shift depends on the inter-particle spacing. The closer the nanoparticles are, the stronger the coupling between the neighboring particles is and thus the larger the red shift in optical spectrum. This is a well-known behavior that has been observed in dimers[9] and is also consistent with the effective medium analysis presented later. In the optical extinction spectra presented in Fig. 5, **TP** shows by far the largest red shift. In fact, the **TP** spectra in Fig. 4a show that the original extinction peak at 530 nm which was dominant in the monolayer sample became overwhelmed by the fast emerging second peak at a longer wavelength. The position of the second peak exhibited a modest red shift from 640 nm for 2 layer sample to 685 nm for 4 layer sample. In contrast, the **COP-3P** spectra in Fig. 5b show a very small red shift with increasing number of layers to 550 nm for the 4 layer sample. In the **COP-6VP** spectra, the red shift was slightly larger, reaching 560 nm for the 4 layer sample, as shown in Fig. 5c. These observation led us to conclude that the self-assembly with **TP** resulted in the most dense packing of gold nanoparticles with smallest inter-particle spacing, **COP-3P** produced the lowest density gold nanoparticle assembly, and **COP-6VP** slightly higher packing density.

For more quantitative analysis, the extended Maxwell Garnett effective medium theory was used to fit the optical extinction spectra. In this method, the polarizability of individual gold nanoparticle was first calculated by using the Mie theory and then the Maxwell Garnett mixing

rule was used to calculate the complex effective refractive index for the composite structure. It has been shown that the extended Maxwell Garnett effective medium theory provides adequate descriptions of metal nanoparticle clusters by comparing with the rigorous numerical modeling by the multiple scattering method. In order to apply the extended Maxwell Garnett theory, we need to know the gold nanoparticle size, their density inside the self-assembled film and the refractive indexes of gold and the background medium. The average size of the gold nanoparticle was measured to be 14 nm by the scanning electron micrographs (SEMs). The average spacing between the nanoparticles is determined by the cage molecule and was directly measured by a series of transmission electron micrographs (TEMs). As shown in Fig. 6, the TEM images clearly showed the inter-particle spacing was related to the cage molecules used. The bare nanoparticles and **TP**-grafted nanoparticles formed clusters of touching nanoparticles whereas the cage molecule coated nanoparticles clearly showed finite gaps between them. The average spacing between the adjacent nanoparticles was determined by averaging 30~40 inter-particle spacings extracted from a series of TEM images. For **COP-3P**, the gap was measured to be 2.49 ± 0.59 nm and for **COP-6VP** it was 2.66 ± 1.23 nm. These values are in excellent agreement with the cage molecule sizes. From the molecular structure, the transverse size of **COP-3P** defined as the distance between adjacent binding sites was estimated to be 2.73 nm. For **COP-6VP**, since there were six binding sites, the distance between a pair of biding sites varied from 1.5 nm to 3.5 nm. Therefore, the slightly larger average gap size together with larger standard deviation obtained for **COP-6VP** was considered consistent with the molecular structure. We also note that planar linker molecules similar to **TP** were shown to result in touching nanoparticles.[3] We therefore infer that the 3D structure of cage molecules is an important factor in creating finite spacing between nanoparticles.

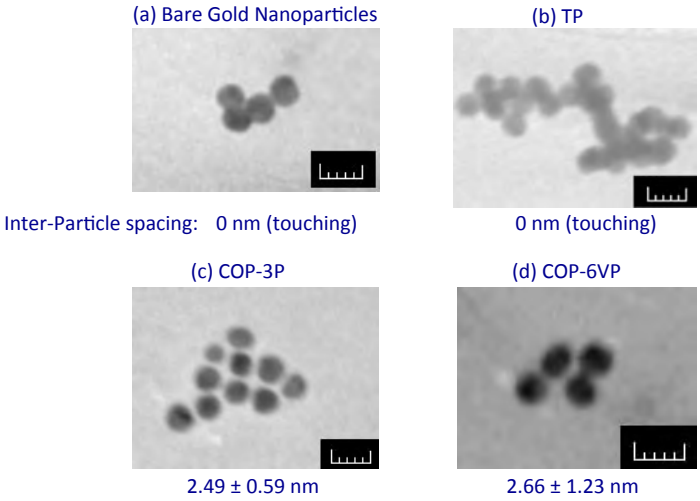

Figure 6. Transmission electron micrographs of gold nanoparticle clusters with various linker molecules: (a) bare nanoparticles, (b) **TP**, (c) **COP-3P** and (d) **COP-6VP**. The scale bars indicate 20 nm.

For the refractive index of gold, we used the experimentally measured dielectric function[10] with slightly increased imaginary part to account for higher loss due to increased scattering in nanoscale geometry as customarily done in plasmonic nanostructure research. The

background medium refers to the space between gold nanoparticles and is composed of cage molecules and air. It was not possible to accurately determine the amount of cage molecules in the space between gold nanoparticles. We therefore measured the refractive index of cage molecule thin films by ellipsometry (Fig. 7) and then used the volume fraction of cage molecules in the background medium as a fitting parameter to fit the experimentally measured optical extinction spectra. In all 6 cases presented in Fig. 8, we were able to obtain excellent fitting with cage molecule volume fraction of 0.4~0.5 in the background medium. We also note that the metamaterial structures self-assembled with **COP-3P** and **COP-6VP** molecules exhibited a small feature in the long wavelength region between 700 and 800 nm. This was attributed to the formation of larger clusters of gold nanoparticles during the drying process introduced between application of cage molecule solution and gold nanoparticle solution. When we kept the samples wet at all times, this long wavelength feature disappeared.

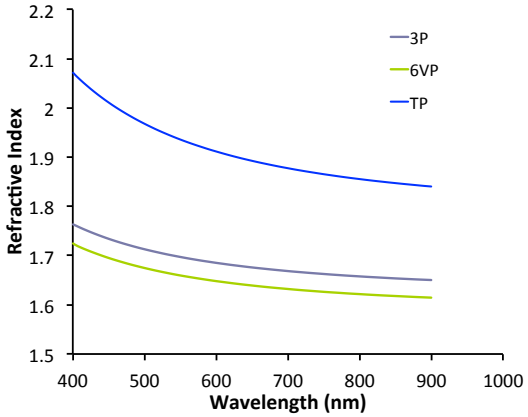

Figure 7. Refractive indexes of thin films of cage molecules measured by ellipsometry

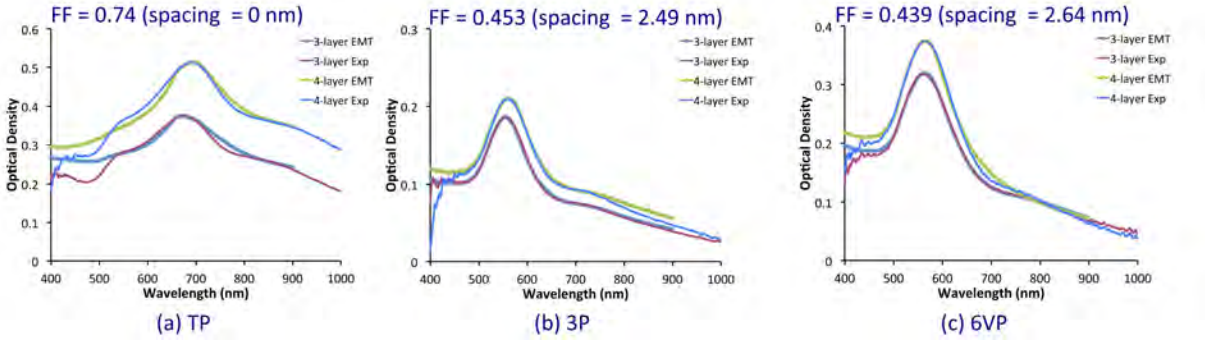

Figure 8. Experimental optical extinction spectra and the effective medium theory fitting for 3-layer and 4-layer self-assembled gold nanoparticle films using (a) **TP**, (b) **COP-3P** and (c) **COP-6VP**

From the fitting by the effective medium theory presented in Fig. 8, effective permittivity can be extracted. The real and imaginary parts of effective permittivity are plotted in Fig. 9. The general features of the effective permittivity were similar in all three cases and in agreement with the classical oscillator model in that the imaginary part exhibited a peak corresponding to the absorption band observed in experiments while the real part showed a wiggle around the resonance. The origin of the resonance is obviously the surface plasmon resonance of individual

gold nanoparticles shifted and broadened through the dipole-dipole interaction taken into account in the extended Maxwell Garnett effective medium theory. While the general behavior was the same for all three samples, a key difference was observed between **TP** and the two cage molecules. The two samples prepared with **COP-3P** and **COP-6VP** showed almost identical dielectric functions for the 3-layer and 4-layer cases while there were large discrepancies in **TP**. Ideally, the same dielectric function should be retrieved irrespective of the sample thickness if the effective medium theory is truly valid. The validity of various effective medium theories has a long history of debate and is well documented.[11] Maxwell Garnett theory or extended Maxwell Garnett theory are generally considered better suited than other approaches such as Bruggeman theory, for the particulate composites as those discussed in this case. Rigorously speaking, the Maxwell Garnett theory should be valid only in the small particle size and small volume fraction limit. However, for small particles, it was shown to be reasonably accurate over a surprising wide range of volume fraction.[12]

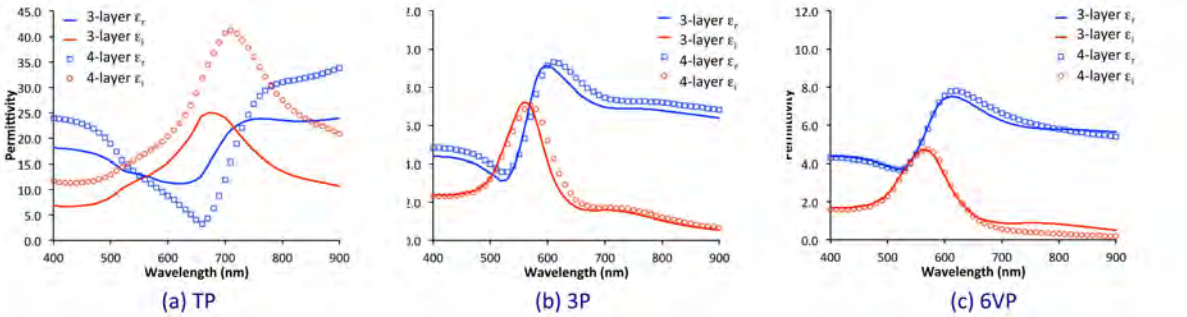

Figure 9. Real (ε_r) and imaginary (ε_i) parts of permittivity extracted from the effective medium theory fitting presented in Fig. 8. 3-layer samples are plotted with solid lines and 4-layer samples were plotted with symbols.

This was once again confirmed by the present study. In the cases of **COP-3P** and **COP-6VP** samples, the fact that almost identical dielectric functions were retrieved for two different thicknesses suggested that meaningful dielectric functions were obtained. The differences between 3-layer and 4-layer cases were only a few percent at most wavelengths and less than 10% even at maximum. The small differences most likely stemmed from the small difference in the background index used to obtain the best fit to the experimental extinction spectra. Since the background index depends on the volume fraction of cage molecules within the gap space between the gold nanoparticles, it is perfectly understandable that there could exist small variations from sample to sample. The large discrepancies between the 3-layer and 4-layer dielectric functions obtained for **TP**, however, indicated the failure of the Maxwell Garnett effective medium theory. This was in fact expected because the Maxwell Garnett theory assumes particulate inclusions in a host medium and is well known to fail to provide the same result when the inclusion and host media are interchanged. Therefore, when the composite structure exhibits an interconnected network topology such as the one exhibited by the touching gold nanoparticles in **TP** samples, the Maxwell Garnett theory is not suitable. This was confirmed by the failure to obtain the same dielectric function for both the 3-layer and 4-layer samples self-assembled by **TP**. If the sample were composed of air "particles" in gold matrix, it would have been possible to use Maxwell Garnett theory by calculating the polarizability of air spheres in gold. However, in

the present case, both gold and air were expected to exhibit network topology and thus the Maxwell Garnett approach was considered simply not applicable.

As further evidence that the retrieved dielectric functions for **COP-3P** and **COP-6VP** samples are meaningful, we conducted numerical simulations using the multiple scattering theory.[13] This is a rigorous approach without any approximation, other than the fact that the spherical wave expansion used to calculate the multiple scattering between spherical inclusions has to be terminated at a finite number, and is therefore a good test for the validity of effective medium approximation. Since the multiple scattering calculation provides the photonic band structure, or the ω-k relationship, we can extract the refractive index from it and compare with the refractive indexes calculated from the effective permittivity given in Fig. 9. The real and imaginary parts of the refractive index calculated by the multiple scattering theory and effective medium theory are shown in Fig. 10. The extinction coefficient, κ, showed excellent agreement for both **COP-3P** and **COP-6VP** samples. For the real part of the refractive index, the effective medium results were slightly smaller than the multiple scattering results but the spectral features such as the wavelengths of local maximum and minimum were in excellent agreement.

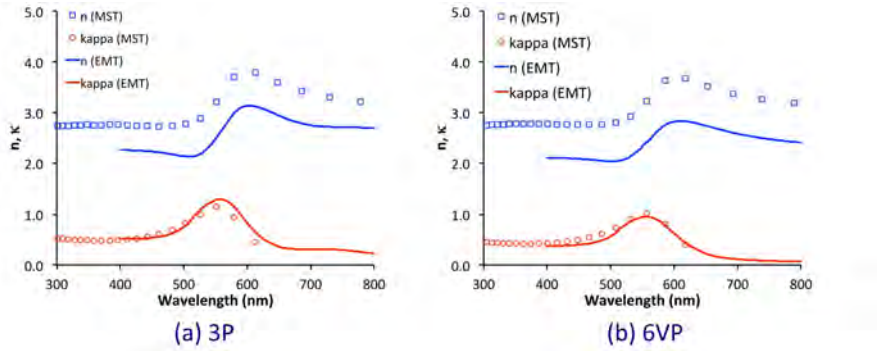

Figure 10. Real (n) and imaginary (κ) parts of refractive index calculated from the effective medium theory (solid lines) and the multiple scattering theory (symbols) for the 4-layer samples prepared with (a) **COP-3P** and (b) **COP-6VP**.

There are two possible reasons for the observed differences. First, the Maxwell Garnett theory was known to underestimate the effective refractive index compared to the rigorous multiple scattering theory.[14] Additionally, the multiple scattering theory assumed perfectly periodic structures whereas the real structures used for experiments and subsequently for fitting by the effective medium theory are random composites. In our calculations, we assumed face-centered cubic arrangements of gold nanoparticles with inter-particle spacing of 2.49 nm for **COP-3P** and 2.64 nm for **COP-6VP** samples, as determined by the TEM images. It is therefore naturally expected that the multiple scattering results would not precisely predict the experimental data. The degree of disagreement would depend on various aspects of the composite structure. In a study of disordered silicon-air photonic crystal structures, Yannopapas showed that the discrepancies in effective permittivity become more significant for large volume fractions and also for large dielectric contrast between the spheres and background medium.[15] For silicon spheres in air, the difference of effective permittivity between ordered and disordered structures reached ~15% for volume fractions comparable to our systems. Given that gold nanoparticle would even more strongly interact with light due to surface plasmon resonance, the observed difference of 20~25% in refractive index between the multiple scattering theory and

effective medium theory is considered reasonable. Finally, we did not conduct multiple scattering calculations for the **TP** samples because the numerical instability prevented us from simulating touching spheres and also because the validity of effective medium description itself was in question as discussed before.

The main result reported in this part of the report is the fact that the experimentally measured optical extinction spectra could be fitted very well with the effective medium theory using the inter-particle spacing measured by TEM. The subsequent discussions further showed that the effective medium results were reliable. From this, we could conclude that we were able to accurately control the inter-particle spacing in the self-assembled film by the choice of cage molecules. Inter-particle spacing is a critical parameter that dictates the coupling between the plasmon resonances and thus ultimately determines the effective dielectric function of the self-assembled structure. The capability of controlling the inter-particle spacing down to the nanometer scale affords us the ability to finely control the dielectric function of the self-assembled artificial structured materials.

3. Template Synthesis of Gold Nanoparticles with an Organic Molecular Cage

In the previous section, we demonstrated precise control of inter-particle spacing in self-assembly gold nanoparticles using molecular cages. For complete control of not only the inter-particle spacing but also the symmetry of assembled nanoparticles, we adopted the nanoparticle-in-cage approach. In this approach, molecular cages that can accommodate one or more nanoparticles inside their intrinsic pores will be developed. The molecules will also have prescribed reactive sites on the outside of the cages. Subsequent crosslinking of these cage-nanoparticle complexes would provide cage-based framework materials in which metal nanoparticles are positioned in a highly ordered fashion in 3D (Fig. 11). It should be noted that we have completely separated the packing motifs, which control the assembly process, from the functional nanoparticles, which ultimately determine the macroscopic material properties. Therefore, the packing motifs are freely tunable and can be designed independently of the properties of nanoparticles they assemble. This approach enables by-design self-assembly of many different crystal structures including highly complex structures such as the diamond structure. It would also be possible to assemble non-symmetric particles like nanorods or nanoplatelets into a highly ordered structure, producing strongly anisotropic materials.

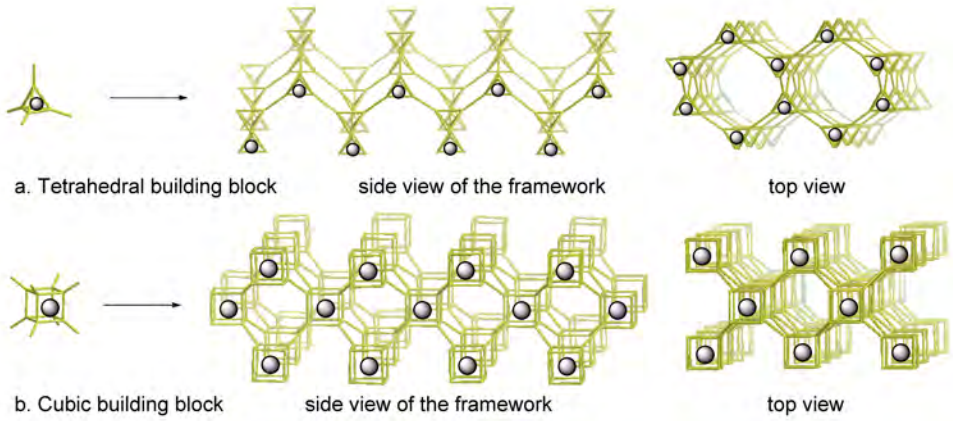

Figure 11. Cage-based framework materials containing metal nanoparticles positioned in 3D crystal lattices.

The first step in the nanoparticle-in-cage approach is to obtain cage molecules containing nanoparticles inside. To accomplish this, we developed template synthesis method where gold nanoparticles were synthesized inside and contained by cage. Compared to conventional monodentate ligands,[16] which form thick insulating layers on the gold nanoparticle (Au NP) surface, cage molecules with multiple internal binding sites can not only serve as a protecting shell with minimum coverage but also control the growth of Au NPs with spatially confined cavity that is large enough to accommodate nanoparticles. Au NPs of a certain size is expected to grow inside the cage, leading to the formation of a core/shell structure: with Au NP as the core and cage molecule as the shell. As a proof-of-concept, we designed trigonal prismatic cage **COP-1** with internal cavity size of 1.8-2.1 nm (Fig. 12), the interior of which is functionalized with three thioether groups. We chose to use thioether as the nucleation site for the Au deposition, since it has higher stability than thiol yet is known to coordinate, albeit weakly, gold colloids.[17-19] Previously reported cage **COP-2** with the same cavity size but lack of thioether anchoring groups was selected as a control compound.[5] We chose triamine 3 as the top and bottom panels and dialdehyde 4 as the three lateral edges. Triamine 4 was prepared as previously described in the literature.[4] Dialdyhyde 4 was synthesized starting with 3,5-diiodo-p-cresol 5, which was prepared from p-cresol. Following alkylation of compound 5, trimethylsilyl protected terminal acetylenes were introduced before radical bromination at the methyl position. The brominated intermediate is critical in that it allows for the later introduction of pendant interior thioether groups. Desilylation of compound 7 followed by the Sonogashira coupling with 3-iodo-benzaldyhyde gave the lateral side piece 4. Imine condensation between the two building blocks 3 and 4 and subsequent reduction led to the formation of **COP-1** that was characterized by 1H NMR, gel permeation chromatography (GPC), and MALDI-MS.

We used a similar two-phase liquid-liquid approach as reported by Brust et al, with tetraoctylammonium bromide (TOAB) as a phase-transfer reagent, to prepare cage-encapsulated gold nanoparticles.[20] A solution of TOAB in CH_2Cl_2 was added to an aqueous solution of $HAuCl_4$ (10 equiv) and stirred until the aqueous layer was colorless, indicating all $AuCl_4^-$ was transferred to the organic phase. A solution of **COP-1** (1 equiv) in CH_2Cl_2 was added to the above biphasic mixture. Upon mixing, no obvious color change was observed in the organic phase. The mixture was subsequently reduced with an aqueous solution of sodium borohydride (200 equiv, rt). The organic phase immediately changed the color from orange-red to dark brown without any precipitates, indicating the efficient Au^{3+} reduction and further stabilization of the resulting Au NPs by cage molecule **COP-1**. The organic layer containing AuNP@**COP-1** complex was separated, and AuNP@**COP-1** complex was precipitated out from ethanol and collected by centrifugation. The resulting AuNP@**COP-1** complex was soluble in all organic solvents and stable in solutions, with no evidence of agglomeration, and without noticeable color change, over periods of several weeks. The Au NPs were characterized by UV-Vis and transmission electron microscopy (TEM).

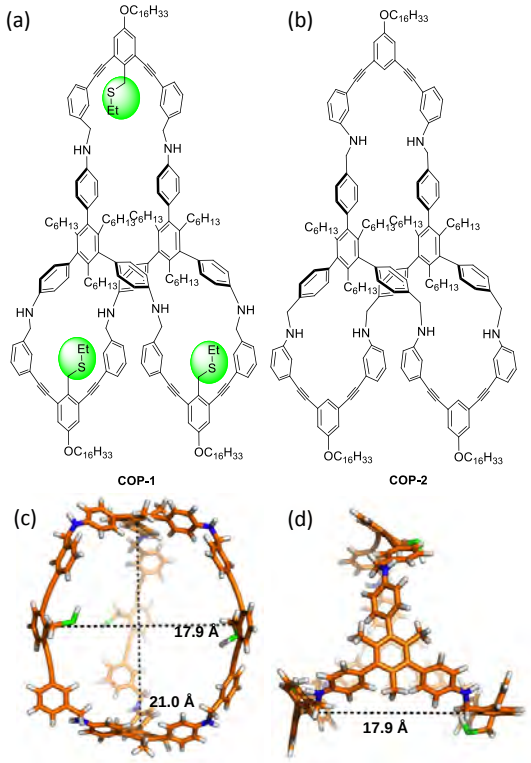

Figure 12. Structures of **COP-1** (a), **COP-2** (b), and fully stretched model of **COP-1**: the side view (c), and the top view (d). Methyl group and hydrogen were used in the calculation instead of hexyl and $OC_{16}H_{33}$ groups respectively for simplification.

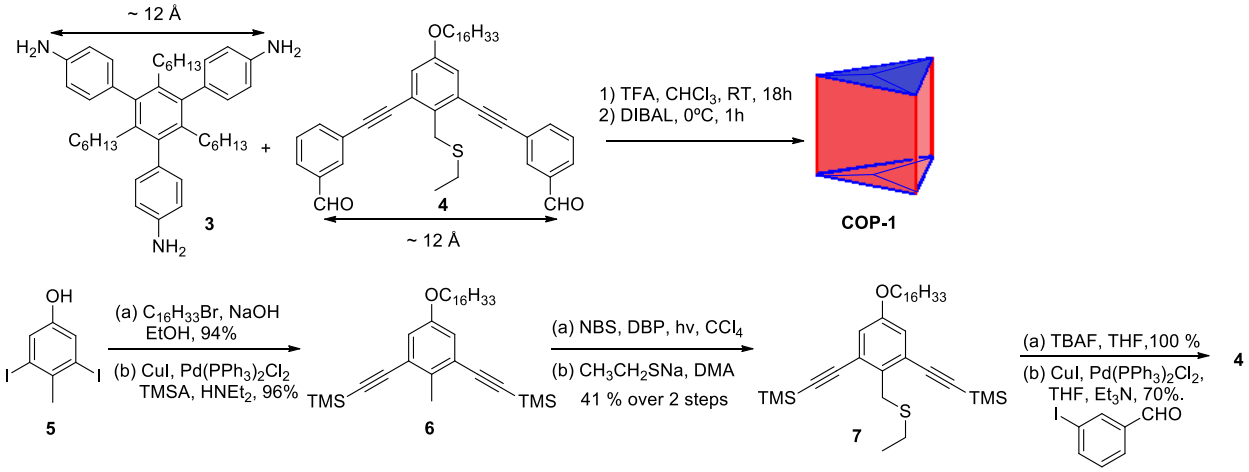

Scheme 1. Synthesis of molecular cage **COP-1**.

UV-Vis absorption spectrum of the solution before and after reduction is shown in Fig. 13c. All the absorption was measured in CH_2Cl_2 at the same concentration (1.4 μM). In the absence of **COP-1**, the absorption spectrum of tetrabutylammonium tetrachloroaurate(III) in CH_2Cl_2 shows absorption peaks at λ = 250 nm, and 380 nm, arising from the ligand-to-metal charge-transfer (LMCT) transition (dotted line, Fig. 13c). Upon the addition of the cage

molecule to the Au^{3+} solution, the absorption of **COP-1** appeared as a shoulder band in the region around 275-381 nm, and the intensity of the peak at 380 nm was decreased (AuCl4@**COP-1**, green line, Fig. 13c). The disappearance of the 250 nm band and the emergence of featureless broad tail extending up to 700 nm after the reduction indicates the complete reduction of $AuCl_4^-$ to zerovalent Au and the formation of gold nanoparticles with diameter less than 2 nm. Despite their small size, we did not observe any signs of aggregation even after several weeks in solution, supporting the notion that nanoparticles reside inside the cage cavity. The particle diameter and size distribution were analyzed based on the TEM images. All the samples were prepared using a solution of AuNP@**COP-1** in CH_2Cl_2. The solution was drop cast on the carbon-coated 300 mesh copper grids (CF300-Cu), and allowed to air dry before the measurements. The TEM image (Fig. 13a) of AuNP@**COP-1** showed the formation of well-dispersed Au NPs with the average diameters of 1.9 nm.

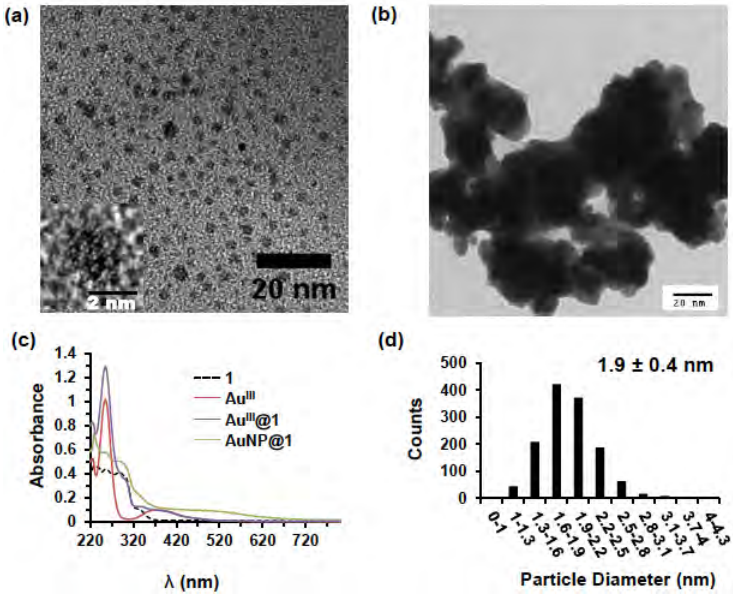

Figure 13. TEM micrographs (scale bar 20 nm) of AuNP@**COP-1** complex (a) and AuNP@**COP-2** complex (b); UV-Vis absorption spectra of gold complexes in CH_2Cl_2 (c); the size distribution of AuNP@**COP-1** complex (d).

In order to further investigate the role of cage scaffold and thioether groups in Au NP synthesis, we conducted two control experiments using **COP-2** that is lack of thioether groups, and thioether ligand 4 that is lack of a cavity. First, $HAuCl_4$ was reduced in the presence of **COP-2**, a structural analog of **COP-1** but without the three internal thioether groups. As expected, upon reduction with $NaBH_4$, we observed the immediate and complete precipitation of aggregated NPs under the similar conditions. The TEM image of Au NPs obtained from the control experiment with **COP-2** (Fig. 13b) showed only shapeless agglomerates, indicating that **COP-2** is unable to serve as a template for the synthesis of Au NPs, presumably due to the lack of nucleation (i.e. Au binding) sites. In another control experiment, when the side piece 4 bearing a thioether group was used as the ligand, we observed similar rapid aggregation and precipitation

of Au NPs upon reduction, suggesting the poor stabilization of Au NPs by a monodentate open ligand 4. It is therefore tempting to conclude that both the thioether groups and the closed cage structure itself are playing critical roles in controlled Au NP synthesis. The thioether groups serve as the initial nucleation sites for Au NP growth and also stabilize the resulting nanoparticle. Once seeded, the Au nanocluster grows until it is confined sterically within the cage, and the three thioether groups and the six amino groups provide stabilization through Au surface binding. The fact that the AuNP@**COP-1** complexes themselves remain isolated from one another is likely due to the long alkyl chains present around the cage exterior. The working mechanism of this cage-template is very different from that of the previously reported dendrimer-template, which inherently relies on multipoint interactions that conform to the surface of particle thus allowing it to grow until 'dendritic wrapping' of the cluster becomes favorable.[21]

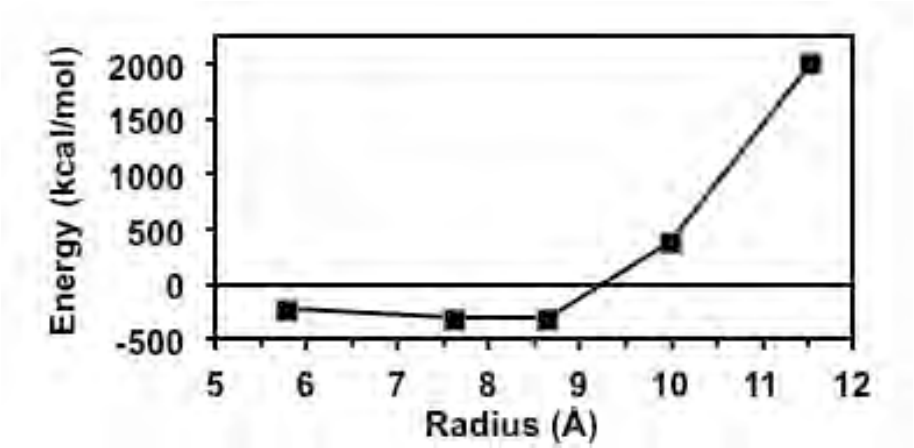

Figure 14. Energy of **COP-1** as a function of encapsulated nanoparticle radius.

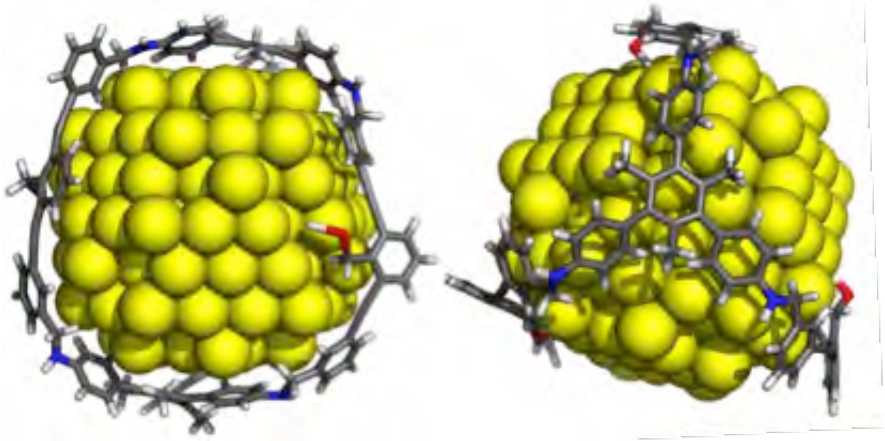

Figure 15. Calculated energy-minimized structure of AuNP@**COP-1**. Au NP radius is 8.65 Å.

To rationalize our experimental findings, we used computational simulation to model the interaction between **COP-1** and Au NPs of different radii. The Au NPs were generated using cubic close-packed lattice of gold crystal structure with a closest Au-Au separation at 0.2884 nm. Five different Au NPs are used, with radii of 11.54, 9.99, 8.65, 7.63, and 5.77 Å respectively. For each nanoparticle, we built a cage around it and bonded the three sulfur atom of the cage to the gold atoms at the equator of the nanoparticle, 120° apart. The Amber 11.0 molecular dynamics program package[22] was then used to optimize the structures of the cage/nanoparticle complexes. The force field used for the cage was the general Amber force field (GAFF field)[23] with the charge parameters computed by AM1-BCC method.[24] For each optimization run, the atoms on gold nanoparticle were frozen and the structure of the cage was optimized. The cage was first minimized for 5000 steps using the conjugate gradient method, and then it was further optimized by simulated annealing method for 150 picoseconds with a time-step of 1 femtosecond. During the simulated annealing, the system temperature was first raised up to 1000 K for 50 picoseconds and then gradually cooled to 0 K for another 100 picoseconds. Finally, the annealed structure was minimized again for another 5000 conjugate gradient steps. The total energy of cage-cage and cage-gold interactions was calculated based on the energy-minimized structure. Fig. 14 shows the cage energy as a function of the encapsulated nanoparticle radius. The energy first decreases when the radius increases due to the larger van der Waals attraction between the cage and the nanoparticle. At a radius between 7.63 and 8.65 Å the energy reaches the minimum and the structure of the AuNP@**COP-1** complex is presented in Fig. 15. This is in very close agreement with the 1.4 ± 0.4 nm average diameter we observed experimentally through the TEM characterization. When the nanoparticle radius is further increased, the cage has to stretch to accommodate the particles, causing the rapid increase in energy.

The key result of this study is that small Au NPs with narrow particle size distribution (1.9 ± 0.4 nm) can be formed inside the cavity of an organic cage molecule. To the best of our knowledge, this is the first example of in situ Au NP growth in a confined

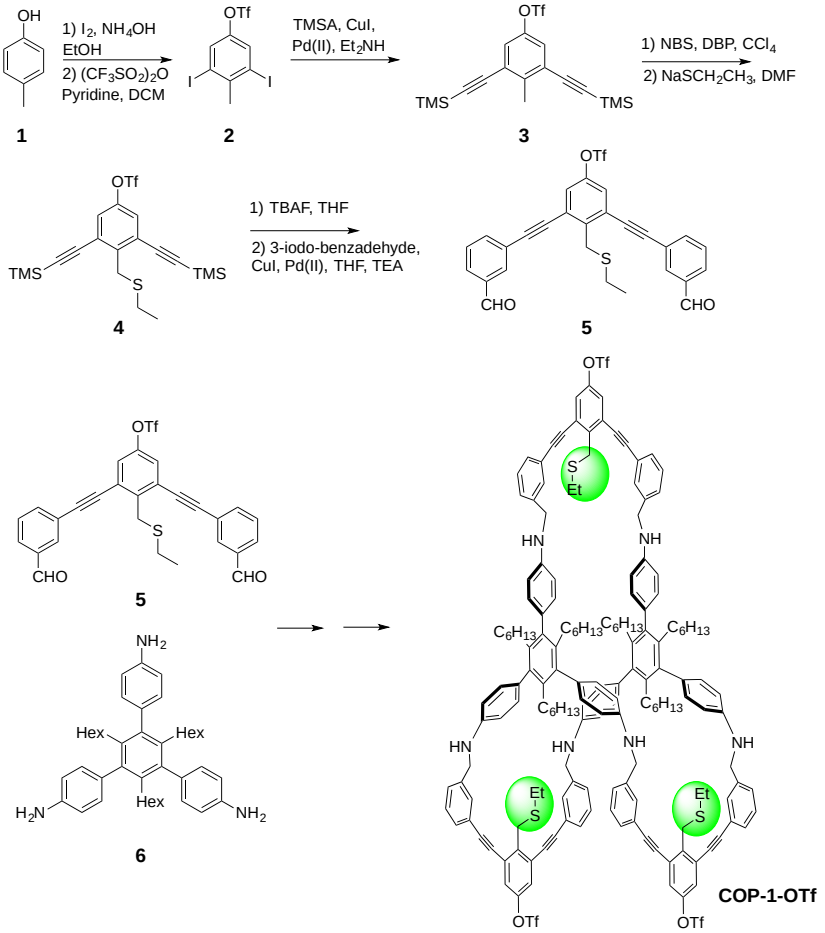

Figure 16. Synthesis of molecular cage substituted with OTf reactive sites (directing groups).

organic molecular environment. Moreover, the average particle size obtained from this cage-templated synthesis is consistent with the molecular dynamics simulation results. The work reported herein would guide future rational design of particles of various sizes, and also possibly of different shapes.

4. Synthesis of cage molecules with linking (directing) groups

Having demonstrated the synthesis of gold nanoparticles in cage molecules, the next step is to demonstrate directed self-assembly of AuNP-cage complexes. For this purpose, directing groups (reactive sites) need to be installed on the exterior of the cage compounds. In this way, the cross-linking between molecular cages would lead to the ordered assembly of encapsulated nanoparticles. As a proof-of-concept, we proposed a molecular cage (**COP-1-OTf**) containing three triflate groups (OTf) on its side arms that are known to be able to go through cross-coupling reactions with either terminal acetylenes or arylboronic acids. The synthesis starts from the commercially available *p*-cresol. Iodination of **1** followed by the triflic acid anhydride treatment provided intermediate **2**, which was further subjected to Sonogashira coupling, bromination and thiolation to provide the thioether intermediate **4**. Final desilylation followed by another Sonogashira coupling with 3-iodobenzaldehyde afforded the side arm building block **5**. The molecular cage (**COP-1-OTf**) synthesis was conducted under the same reaction condition as for the synthesis of **COP-1**. Preliminary study in the imine condensation between **5** and triamine **6** (top and bottom panels) showed some indications that the target cage **COP-1-OTf** (Figure 16) was formed. Next step, we will grow Au NPs inside this molecular cage by following the same procedure as the **COP-1** case we reported in Section 3. Further crosslinking of the cage-NP complexes through the reaction at OTf sites would lead to ordered assembly of Au nanoparticles.

Given the relatively more labile nature of the OTf group, which may be cleaved during the cage formation and thus decrease the efficiency of further cross-coupling, we have also explored introducing more robust directing groups onto the cage exterior. We have proposed a series of cages that utilize the same side arm building block used in **COP-1** but instead have incorporated a tetrahedral top piece building block functionalized with various R groups (R_{a-c}) to give target cages COP-2_{a-c}. The synthesis of each tetrahedral building block starts with the tricarboxylic acid **7** which then undergoes a curtius rearrangement to give triamine $\mathbf{8}_a$. Triamines $\mathbf{8}_{b,c}$ can then be synthesized from triamine $\mathbf{8}_a$ simply by transforming the iodine into the desired functional groups (Figure 17), each of which allows for the opportunity to explore the 1-dimensional (1D) ordered assembly of nanoparticles using a different chemistry.

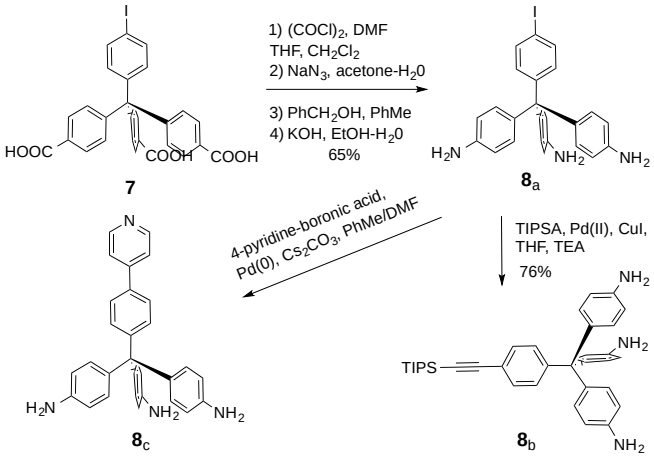

Figure 17 Synthesis of triamine top pieces with various R-directing groups.

The molecular cages (**COP-2**$_{a\text{-}c}$) can be synthesized under the same reaction condition as for the synthesis of **COP-1** (Figure 18). Thus far we have successfully synthesized both **COP-2**$_a$ and **COP-2**$_b$, with both cage structures being confirmed by ^{1}H NMR and mass spectrometry. Furthermore, the cage-templated nanoparticle synthesis using both **COP-2**$_a$ and **COP-2**$_b$ to give AuNP@**COP-2**$_a$ and AuNP@**COP-2**$_b$, respectively, has been confirmed by TEM and UV/Vis. By using AuNP@**COP-2**$_a$ we have been exploring the ordered assembly of the nanoparticles through the cross-coupling of the iodine unit and a simple diethynylbenzene linker through Sonogashira coupling reaction (Figure 19). There is indication that the polymerization does occur and furthermore we have observed some semblance of trimer formation in the TEM images (Figure 20). The optimization of this reaction is still in progress in order to generate longer chains in larger populations. The AuNP@**COP-2**$_a$ complex utilizes a TIPS-protected terminal acetylene that can be removed using a TBAF deprotection protocol and then further homocoupled into a 1D polymer using CuCl catalyzed Glaser-Hay coupling reaction.

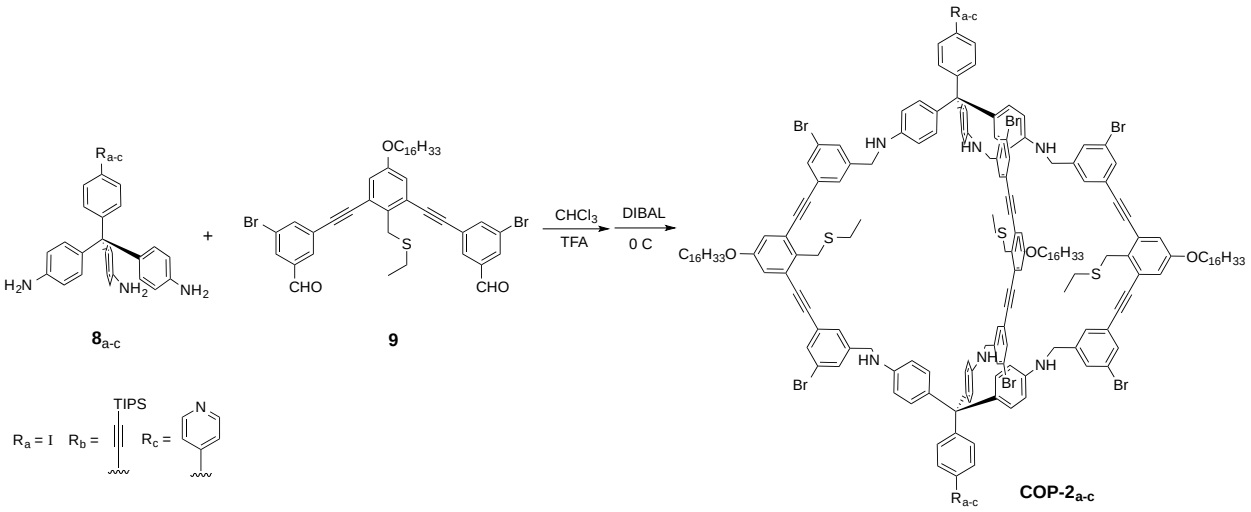

Figure 18. Synthesis of molecular cages substituted with various R-directing groups.

This method offers the ability to perform the nanoparticle synthesis and its subsequent polymerization in an one-pot reaction. Additionally, it is possible that the growth of the polymer chain can be monitored by UV/Vis given the extension of the π system. This system is still being explored as another potential route to covalent assembly of nanoparticles in a 1D chain. We also have in mind a cage that uses building block **8**$_c$, which is terminated with a pyridine unit, in order to explore non-covalent self-assembly. We envision that it is also possible to direct the nanoparticles using a coordination chemistry approach through the addition of a palladium based ligand, PdX_4. The synthesis of **8**$_c$ is still in progress but there is indication that the synthesis is promising.

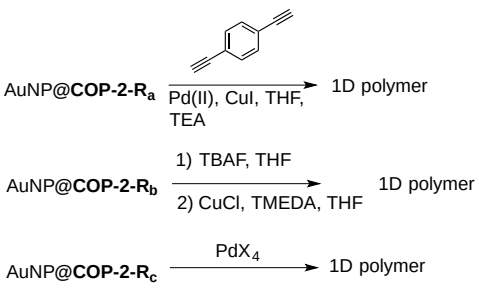

Figure 19. Strategies to generate 1D nanoparticle polymers using various AuNP@COP architectures.

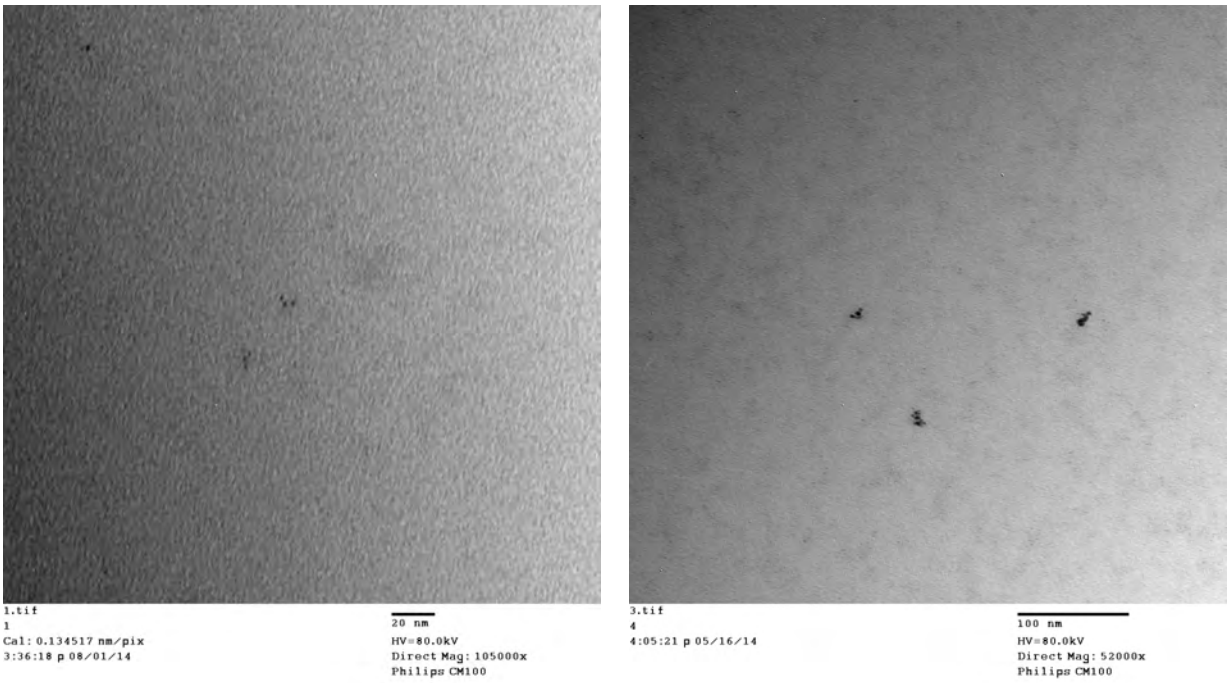

Figure 20. TEM images of AuNP@cage based oligomers.

5. DNA-based cages – new approach for large sized molecular cages and nanoparticles

Although the above design strategy based on purely organic building blocks works well for the synthesis of a few nanometer-sized nanoparticles, it will take much more synthetic efforts to prepare even larger molecular cages for the synthesis of NPs with diameters of tens of nanometers. To achieve more efficient host compound preparation for the template synthesis of NPs, DNA-organic hybrid molecular cages are considered as promising candidates for preparation of large sized nanoparticles. As the first prototypical molecule, a cubic-shaped hybrid cage structure is proposed. The tetraarylmethane (Figure 21b) will be used as the vertex building block. A single strand DNA will be attached to the end of each arm through well established procedure (amide formation). Then the other DNA strand with complementary binding sites to the first one will be installed on both ends of a linker molecule. Then upon these two DNA strand binding, a cubic-shape molecular cage can be constructed (Figure 21a). Depending on the geometry and combination of different building blocks, a tetrahedral-shape cage can also be constructed. The NP binding sites will be installed on the cage building blocks (corner pieces, thioether groups, (Figure 21b) or on the linkers, which would serve as the nucleation sites for the NP growth. The size of the NP will be controlled by the cage physical dimension, which can be easily tuned by varying the length of the base pairs in the DNA strands. Once the hybrid cage-encapsulated nanoparticles are obtained, further self-assembly or covalent linking of the molecular cages through the reactive sites (directing groups, installed on each vertex of the cage) would lead to cage-NP composites, with NPs distributed in an ordered fashion in three dimension, mimicking the crystal lattice shown in Figure 11b.

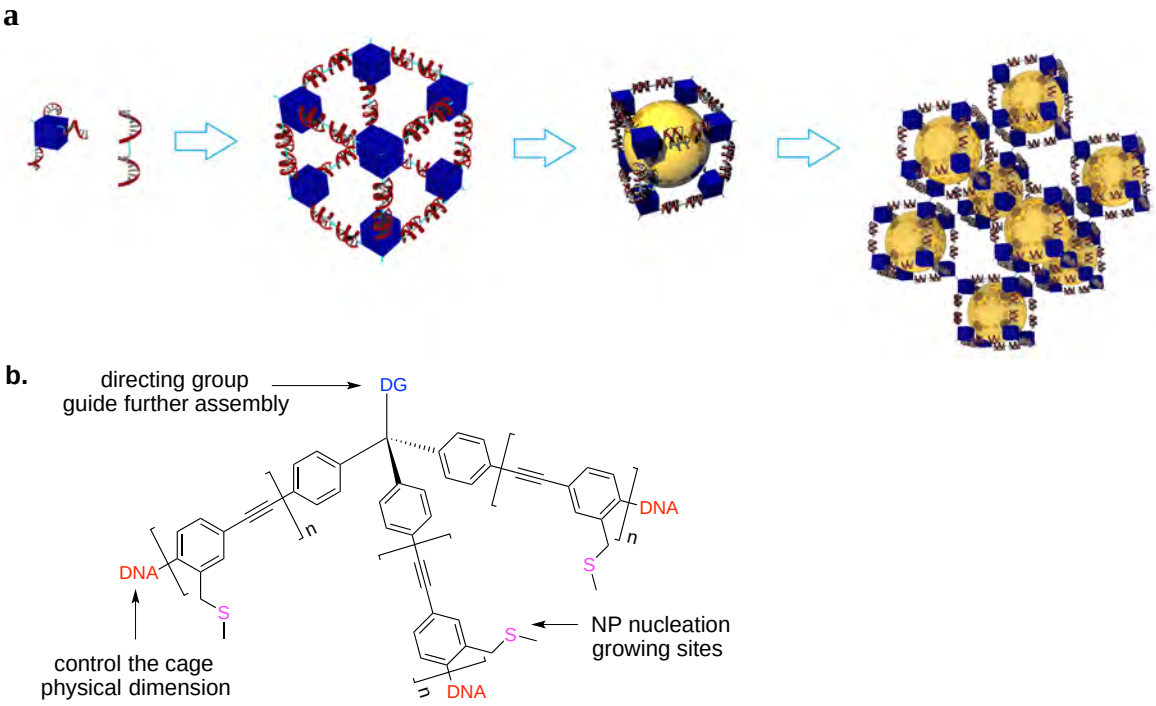

Figure 21. a) the modeling of DNA linked molecular cage with NP bound inside. b) the chemical structure of the proposed corner building block for the molecular cage construction.

The proposed synthetic route for the DNA-organic hybrid molecular cage starts with 4-tritylaniline, which can be prepared by refluxing a solution of aniline and commercially available tritylchloride. After nitration of the trityl group, the amine is then protected with a simple amide using acetyl chloride. This group is robust enough to withstand most chemical reactions but can also be removed in order to direct the DNA-organic hybrid molecular cage later in the synthesis. Once protected, the nitro groups are then converted to amines using $SnCl_2$ reduction and replaced with iodo groups, which then allows for the arms of the building block to be extended as needed using a series of Sonogashira coupling reactions. After the iodo groups are replaced with TMS protected acetylenes and deprotected with K_2CO_3, either 4-iodo-benzadehyde or 4-iodo-benzoic acid can be attached to give, respectively, the trialdehyde or the tricarboxylic acid (Figure 22).

We have experimented with attaching a strand of DNA to the trialdehyde tetrahedral piece through the use of hydrazone chemistry in a mixture of water and DMF. We found that in the beginning of the reaction the organic tetrahedral piece was insoluble, but after overnight reaction the solution became homogenous and contained no precipitation. Though we still need to confirm the DNA attachment using mass spectrometry, this result represents a very encouraging indirect evidence supporting the successful attachment of the DNA to the corner piece unit. Currently we are also exploring another method for DNA attachment involving the addition of an NHS ester to the tricarboxylic acid to give a tri-NHS-substituted corner piece. This compound study is still in progress but the synthesis is very promising.

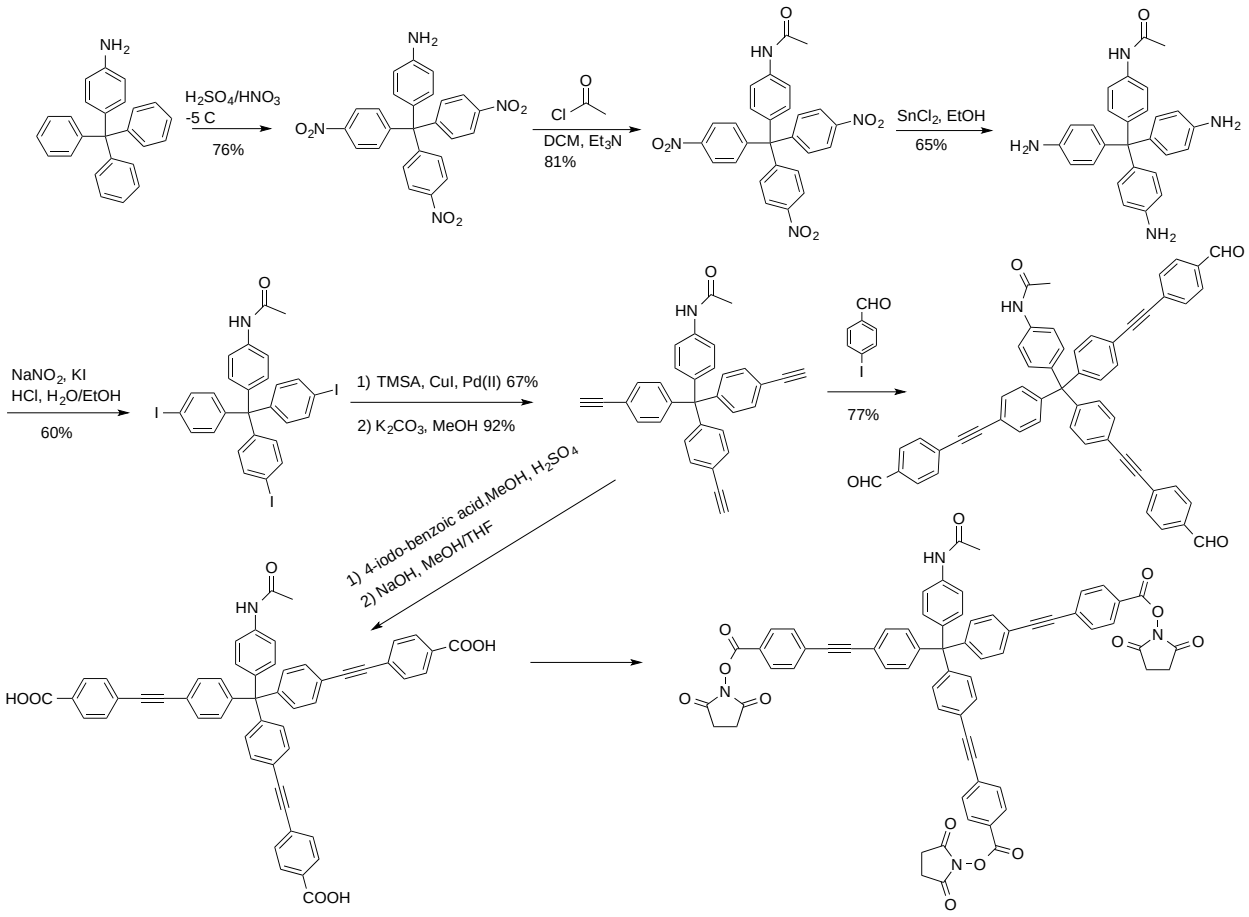

Figure 22. Synthesis of tetrahedral building blocks for DNA-organic hybrid molecular cages.

6. Bibliography

1. Bilić, A., Reimers, J. R. & Hush, N. S. Adsorption of Pyridine on the Gold(111) Surface: Implications for 'Alligator Clips' for Molecular Wires. *J. Phys. Chem. B* **106,** 6740–6747 (2002).
2. Quek, S. Y. *et al.* Mechanically controlled binary conductance switching of a single-molecule junction. *Nature Nanotech* **4,** 230–234 (2009).
3. Kaminker, R. *et al.* Molecular Structure-Function Relations of the Optical Properties and Dimensions of Gold Nanoparticle Assemblies. *Angewandte Chemie International Edition* **49,** 1218–1221 (2010).
4. Jin, Y., Voss, B. A., Noble, R. D. & Zhang, W. A Shape-Persistent Organic Molecular Cage with High Selectivity for the Adsorption of CO2 over N2. *Angewandte Chemie* **122,** 6492–6495 (2010).

5. Zhang, C., Wang, Q., Long, H. & Zhang, W. A Highly C 70Selective Shape-Persistent Rectangular Prism Constructed through One-Step Alkyne Metathesis. *J. Am. Chem. Soc.* **133,** 20995–21001 (2011).
6. Yu, A., Liang, Z., Cho, J. & Caruso, F. Nanostructured Electrochemical Sensor Based on Dense Gold Nanoparticle Films. *Nano Lett.* **3,** 1203–1207 (2003).
7. Joseph, Y. *et al.* Self-Assembled Gold Nanoparticle/Alkanedithiol Films: Preparation, Electron Microscopy, XPS-Analysis, Charge Transport, and Vapor-Sensing Properties †. *J. Phys. Chem. B* **107,** 7406–7413 (2003).
8. Cunningham, A., Mühlig, S., Rockstuhl, C. & Bürgi, T. Coupling of Plasmon Resonances in Tunable Layered Arrays of Gold Nanoparticles. *J. Phys. Chem. C* **115,** 8955–8960 (2011).
9. Atay, T., Song, J.-H. & Nurmikko, A. V. Strongly Interacting Plasmon Nanoparticle Pairs: From Dipole−Dipole Interaction to Conductively Coupled Regime. *Nano Lett.* **4,** 1627–1631 (2004).
10. Johnson, P. B. & Christy, R. W. Optical constants of the noble metals. *Phys. Rev. B* **6,** 4370 (1972).
11. Milton, G. W. The theory of composites. **6,** (2002).
12. Tamma, V. A., Lee, J. H., Wu, Q. & Park, W. Visible frequency magnetic activity in silver nanocluster metamaterial. *Appl Opt* **49,** A11–A17 (2010).
13. Stefanou, N., Yannopapas, V. & Modinos, A. MULTEM 2: A new version of the program for transmission and band-structure calculations of photonic crystals. *Computer physics communications* **132,** 189–196 (2000).
14. Moroz, A. & Sommers, C. Photonic band gaps of three-dimensional face-centred cubic lattices. *J. Phys.: Condens. Matter* **11,** 997 (1999).
15. Yannopapas, V. Effective-medium description of disordered photonic alloys. *J. Opt. Soc. Am. B* (2006).
16. Kim, Y.-G., Oh, S.-K. & Crooks, R. M. Preparation and Characterization of 1−2 nm Dendrimer-Encapsulated Gold Nanoparticles Having Very Narrow Size Distributions. *Chem. Mater.* **16,** 167–172 (2004).
17. D'Al o, A. *et al.* Oligothia Dendrimers for the Formation of Gold Nanoparticles. *Adv. Funct. Mater.* **14,** 1167–1177 (2004).
18. Li, X.-M. *et al.* Formation of gold colloids using thioether derivatives as stabilizing ligands. *J. Mater. Chem.* **11,** 1919–1923 (2001).
19. Peterle, T. *et al.* Multidentate thioether ligands coating gold nanoparticles. *Chem. Commun.* 3438 (2008). doi:10.1039/b802460j
20. Brust, M., Walker, M., Bethell, D., Schiffrin, D. J. & Whyman, R. Synthesis of thiol-derivatised gold nanoparticles in a two-phase Liquid-Liquid system. *J. Chem. Soc., Chem. Commun.* 801–802 (1994). doi:10.1039/c39940000801
21. Hermes, J. P. *et al.* Gold Nanoparticles Stabilized by Thioether Dendrimers. *Chem. Eur. J.* **17,** 13473–13481 (2011).
22. Case, D. A. *et al.* AMBER 11, 2010. *University of California, San Francisco* (2010).
23. Wang, J., Wolf, R. M., Caldwell, J. W., Kollman, P. A. & Case, D. A. Development and testing of a general amber force field. *J. Comput. Chem.* **25,** 1157–1174 (2004).
24. Jakalian, A., Bush, B. L., Jack, D. B. & Bayly, C. I. Fast, efficient generation of high-quality atomic charges. AM1-BCC model: I. Method. *J. Comput. Chem.* **21,** 132–146

(2000).